Inorganic Chemistry

pubs.acs.org/IC

Article

Influence of Triazole Substituents of Bis-Heteroleptic Ru(II) Probes toward Selective Sensing of Dihydrogen Phosphate

Sahidul Mondal, Koushik Sarkar, and Pradyut Ghosh*

Cite This: *Inorg. Chem.* 2021, 60, 9084−9096

Read Online

ACCESS | Metrics & More | Article Recommendations | Supporting Information

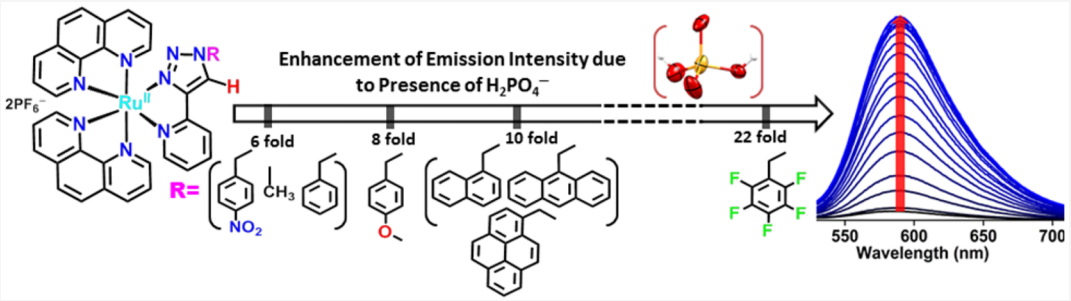

ABSTRACT: A series of seven new bis-heteroleptic Ru(II) probes ($\mathbf{1}[PF_6]_2$−$\mathbf{7}[PF_6]_2$) along with two previously reported probes ($\mathbf{8}[PF_6]_2$ and $\mathbf{9}[PF_6]_2$) containing a similar anion binding triazole unit (hydrogen bond donor) functionalized with various substituents are employed in a detailed comparative investigation for the development of superior selective probes for $H_2PO_4^-$. Various solution- and solid-state studies, such as ^{1}H-DOSY NMR, dynamic light scattering (DLS), single-crystal X-ray crystallography, and transmission electron microscopy (TEM), have established that the selective sensing of $H_2PO_4^-$ by this series of probes is primarily due to supramolecular aggregation driven enhancement of ^{3}MLCT emission. Intestingly, $\mathbf{1}[PF_6]_2$ and $\mathbf{7}[PF_6]_2$, having an electron-deficient (π-acidic) aromatic pentafluorophenyl substituent are found to be superior probes for $H_2PO_4^-$ in comparison to the other aryl- and polyaromatic-substituted analogues ($\mathbf{2}[PF_6]_2$−$\mathbf{6}[PF_6]_2$, $\mathbf{8}[PF_6]_2$, and $\mathbf{9}[PF_6]_2$), in terms of a higher enhancement of the ^{3}MLCT emission band, a greater binding constant, and a lower detection limit. The superiority of $\mathbf{1}[PF_6]_2$ and $\mathbf{7}[PF_6]_2$ could be due to better supramolecular aggregation properties in the cases of pentafluorophenyl analogues via both hydrogen bonding and anion−fluorine/anion−π noncovalent interactions.

INTRODUCTION

Phosphates play vital roles in numerous essential biological as well as environmental processes.[1−14] Thus, the development of superior selective synthetic probes for phosphates are in demand in anion recognition chemistry.[5,13,15−21] During the past few years, several different heterocyclic ring systems containing neutral/cationic N−H/C−H (e.g., urea,[22−26] triazole,[21,24,27−31] imidazole,[32−36] amide,[37−40] pyrrole,[41−45] etc.) moieties containing receptors have been reported for the selective recognition and sensing of phosphates. We have been systematically exploring the ruthenium complexes of pyridine triazole/iodotriazole and phenanthroline toward the development of a new class of metal complex based selective probes and extractants for phosphates.[24,27,46−50] In this regard, initially we developed a bis-heteroleptic Ru(II) probe containing methyl-substituted pyridyl triazole for selective sensing of $H_2PO_4^-$ over $HP_2O_7^{3-}$ and other common inorganic anions through a solitary C−H···anion interaction.[27] Then we introduced a bis-heteroleptic trinuclear Ru(II) probe on a cyanuric acid platform for sensing of higher homologue phosphates (pyrophosphate, ADP, and ATP) over dihydrogen phosphate.[46] Subsequently, we established a superior halogen-bonding-based bis-heteroleptic Ru(II) complex with an iodotriazole-based phosphate sensor that showed metal-assisted second-sphere phosphate binding through solitary XB interactions.[47] Furthermore, our group has explored Ru(II)-polypyridyl-based receptors decorated with various pendant urea moieties for the binding and extraction of phosphates/carboxylates.[24,48,49] In all of the above probes, a wide range of other basic anions do not show any photophysical aspect of sensing behavior. Thus, in this class of probes, the basicity of anions might not govern the anion-sensing selectivity. Our recent investigation has demonstrated that the rigidification of probes via the formation of self-assembly might be responsible for the selective sensing of phosphates.[50] In addition to hydrogen-bonding interactions,

Received: April 8, 2021
Published: June 9, 2021

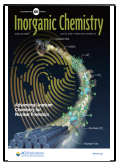

Scheme 1. Synthetic Scheme of Complexes

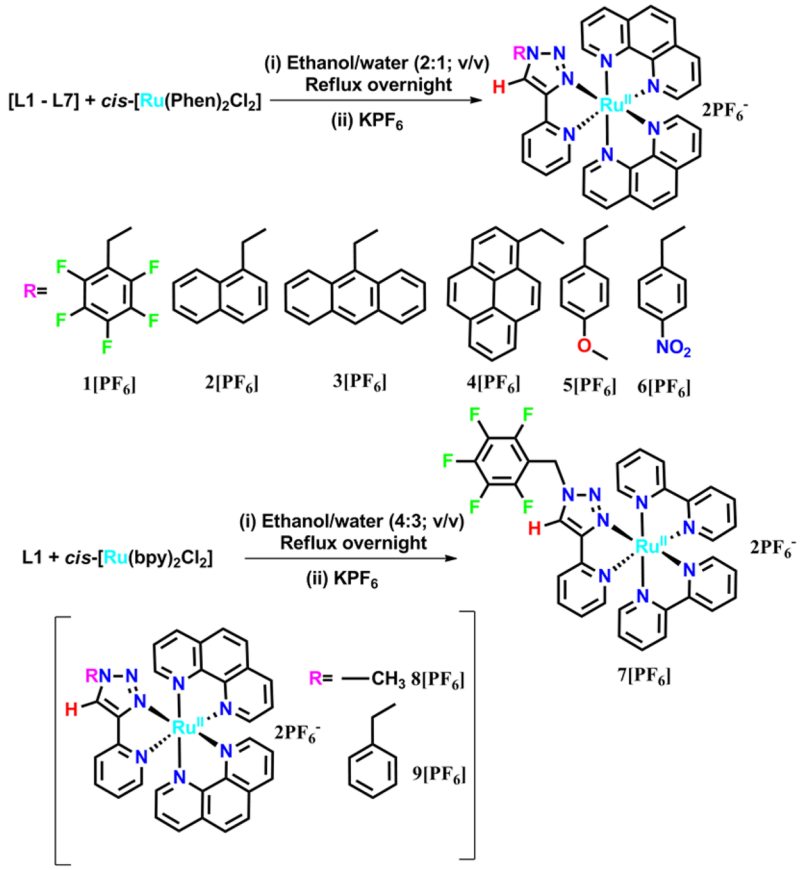

other weak interactions such as $\pi-\pi$ stacking, anion$-\pi$ interactions, etc. also commonly function as noncovalent interactions for the formation of self-assembled structures. Thus, at this juncture, we were curious to systematically develop superior phosphate probes by exploring different substituents on the triazole backbone of bis-heteroleptic Ru(II) complex probes. Thus, herein we report a series of heteroleptic ruthenium probes, ($\mathbf{1}[\mathbf{PF_6}]_2$–$\mathbf{9}[\mathbf{PF_6}]_2$) containing a pyridyl triazole hydrogen bond donor and different pendant (pentafluorophenyl, aryl, polyaromatic) units for a detailed comparative investigation toward the development of superior and selective Ru(II) complex based $H_2PO_4^-$ probes. Moreover, we have generalized the different degrees of enhancement-based selective sensing of phosphate by this series of probes via the selective formation of phosphate-supported extensive self-assembled structures in the solid and solution states.

RESULTS AND DISCUSSION

Designing Strategy and Synthesis of Probes. We have previously shown that bis heteroleptic Ru(II) complexes of triazole ligands ($\mathbf{8}[\mathbf{PF_6}]_2$ and $\mathbf{9}[\mathbf{PF_6}]_2$; Scheme 1) are efficient receptors for selective phosphate sensing via the triazole C–H···anion interaction.[27,46,48] Electronic parameters of the neighboring substituent on the triazole moiety as well as the assembly properties of the substituents might alter the overall acidity of the triazole C–H and self-assembly properties via nonbonding interactions, which might eventually affect the phosphate recognition efficiency of the probes. To account for such effects in the sensing of bis-heteroleptic Ru(II) complexes, we have introduced various substituents comprised of electron-donating, electron-withdrawing, polyaromatic, and electron-deficient (π-acidic unit) groups on the triazole moiety in designing the new probes. Herein we have designed the series of seven bis-heteroleptic ruthenium(II) probes $\mathbf{1}[\mathbf{PF_6}]_2$–$\mathbf{7}[\mathbf{PF_6}]_2$ (Scheme 1), along with the two known complexes $\mathbf{8}[\mathbf{PF_6}]_2$ and $\mathbf{9}[\mathbf{PF_6}]_2$ for a detailed comparative investigation toward selective $H_2PO_4^-$ sensing efficiency. Probes $\mathbf{1}[\mathbf{PF_6}]_2$ and $\mathbf{7}[\mathbf{PF_6}]_2$ contain the same pendant pentafluorophenyl (π-acidic)-substituted triazole; however, they differ in the central core moiety (phenanthroline versus bipyridine). The bis-heteroleptic Ru(II) probes $\mathbf{1}[\mathbf{PF_6}]_2$–$\mathbf{6}[\mathbf{PF_6}]_2$ are prepared in good yields (65–70%) by refluxing of $Ru(phen)_2Cl_2$ and ligands L1–L6 overnight in a binary ethanol/water (2/1) solvent system followed by PF_6^- exchange. The probe $\mathbf{7}[\mathbf{PF_6}]_2$ is synthesized by reacting L1 and $Ru(bpy)_2Cl_2$ in a 4/3 ethanol/water mixture and by anion exchange with good yield (68%) (Scheme 1).

The synthetic procedures of ligands L1–L6 and probes $\mathbf{1}[\mathbf{PF_6}]_2$–$\mathbf{7}[\mathbf{PF_6}]_2$ are detailed in the Supporting Information and the Experimental Section. All of the ligands and complexes have been fully characterized by NMR and mass studies (Figure S1–S57 in the Supporting Information). The observed m/z peaks in ESI-MS (+ve) studies are well-matched with the calculated m/z values for +/2+ charged species of all the complexes. Further, their experimental isotopic distribution patterns and the simulated patterns matched well. Single-crystal X-ray diffraction studies established the structures of all newly synthesized complexes except for $\mathbf{2}[\mathbf{PF_6}]_2$, which are discussed later.

https://doi.org/10.1021/acs.inorgchem.1c01084
Inorg. Chem. 2021, 60, 9084–9096

Table 1. Comparative Photophysical Data of Complexes $1[PF_6]_2$–$7[PF_6]_2$

host	anion	absorbance λ_{max} (nm) (ε (M^{-1} cm^{-1})	emission λ_{max} (nm)	sensing properties: emission intensity enhancement factor	sensing properties: K_a (M^{-1})[a]
$1[PF_6]_2$	none	400 (13005), 440 (10285)	589		
	$H_2PO_4^-$	407 (10775), 449 (9435)	589	22	2.64×10^6
$2[PF_6]_2$	none	402 (13960), 440 (11445)	587		
	$H_2PO_4^-$	402 (11075), 453 (9995)	591	9	7.91×10^5
$3[PF_6]_2$	none	351 (17670), 370 (26595), 391 (34515), 443 (21985)	416		
			438		
			590		
	$H_2PO_4^-$	351 (19990), 370 (23685), 393 (27790), 459 (21085)	416	8	2.63×10^5
			438		
			590		
			608		
$4[PF_6]_2$	none	313 (17835), 327 (26985), 343 (35090), 405 (15080), 443 (12325)	377		
			395		
			417		
			586		
	$H_2PO_4^-$	313 (15155),327 (24080), 343 (32710), 405 (12920), 443 (10320)	377	10	2.14×10^5
			395		
			417		
			636		
$5[PF_6]_2$	none	404 (13355), 443 (10925)	587		
	$H_2PO_4^-$	415 (13255), 459 (12805)	591	8	1.83×10^5
$6[PF_6]_2$	none	403 (12915), 443 (10880)	589		
	$H_2PO_4^-$	415 (14180), 457 (13340)	589	5	4.35×10^4
$7[PF_6]_2$	none	412 (8695), 440 (8960)	597		
	$H_2PO_4^-$	414 (9560), 456 (9900)	597	19	9.26×10^5
$8[PF_6]_2$[27]	none	403 (10850), 445 (8637)	590		
	$H_2PO_4^-$		590	6	5.28×10^4
$9[PF_6]_2$[47]	none	405 (11750), 445 (9250)	585		
	$H_2PO_4^-$	406 (9179), 459 (7873)	590	6	5.56×10^4

[a]Although the 1:1 (H:G) stoichiometry has been adopted to calculate the binding constants here, consideration of both nucleation and aggregation processes should be exercised toward calculating the actual binding constants.

Comparative Phosphate Sensing Properties by Heteroleptic Ru(II) Polypyridyl Complexes in Solution. The probes $1[PF_6]_2$–$6[PF_6]_2$ having the same chromophoric unit show photophysical characteristics in acetonitrile at 298 K similar to those previously observed in $8[PF_6]_2$ and $9[PF_6]_2$. The UV/vis spectral data of $1[PF_6]_2$–$6[PF_6]_2$ are very similar, having intense broad absorption bands centered in the regions of λ_{max} 400–405 nm for Ru(dπ) → phenanthroline and 440–445 nm for Ru(dπ) → pyridine-triazole MLCT charge-transfer transitions (Figure S58 in the Supporting Information). In the case of $7[PF_6]_2$, the UV absorption bands are centered at λ_{max} 412 nm (Ru(dπ) → bipyridine) and 440 nm (Ru(dπ) → pyridine-triazole). In addition, characteristic absorption bands are observed in probes $3[PF_6]_2$ and $4[PF_6]_2$ at λ_{max} 351, 370, and 391 nm for anthracene and λ_{max} 313, 327, and 343 nm for pyrene due to π–π^* transitions. Upon excitation at either of the λ_{max} values of the chromogenic bands, 400 or 445 nm shows a ^{3}MLCT broad luminescence band. On the other hand, upon excitation at λ_{max} 391 and 343 nm for probes $3[PF_6]_2$ and $4[PF_6]_2$, luminescence bands are observed at 416, 438, and 590 nm (for $3[PF_6]_2$) and 377, 395, 417, and 470 nm (for $4[PF_6]_2$) (Figure S58e,g in the Supporting Information). The absorption and emission spectral data of all the probes in acetonitrile are given in Table 1.

All of the probes only show perturbation in the absorption and emission bands with $HP_2O_7^{3-}$ and $H_2PO_4^-$ without any observable change for HSO_4^-, NO_3^-, $CH_3CO_2^-$, HCO_3^-, $C_6H_5CO_2^-$, I^-, Br^-, Cl^-, and F^- anions in acetonitrile at 298 K (Figure 1 and Figure S59 in the Supporting Information). The PL titration of receptors with $TBAH_2PO_4$ was carried out to determine the phosphate-binding stoichiometry with the receptors in acetonitrile at 298 K. The gradual addition of $H_2PO_4^-$ to the probes $1[PF_6]_2$–$6[PF_6]_2$ causes significant perturbations in the emission signal by increasing the intensity of the emission band at λ 585–597 nm. In probes $3[PF_6]_2$ and $4[PF_6]_2$, emission bands that are red-shifted by 15 and 50 nm, respectively, are observed. When the acidity of the triazole C–H is changed by varying the neighboring substituents *p*-$NO_2C_6H_4$, CH_3, C_6H_5, *p*-$OMeC_6H_4$, naphthyl, anthryl, and pyrenyl in probes 5^{2+}, 8^{2+}, 9^{2+}, 6^{2+}, 2^{2+}, 3^{2+}, and 4^{2+} as their hexafluorophosphate salts, respectively, the emission intensity is increased in the range of 5–10-fold only in the presence of $H_2PO_4^-$. In cases of probes 2^{2+}, 3^{2+}, and 4^{2+} as their PF_6^- salts having different polyaromatic substituents, the enhancement of ^{3}MLCT emission is found to be increased with the increase of aromatic rings. Interestingly, in the case of $1[PF_6]_2$ having a pentafluorophenyl substituent, as high as a ~22-fold increase in the emission intensity is observed, which differentiates this probe from the rest of the probes $2[PF_6]_2$–$6[PF_6]_2$, $8[PF_6]_2$,

https://doi.org/10.1021/acs.inorgchem.1c01084
Inorg. Chem. 2021, 60, 9084–9096

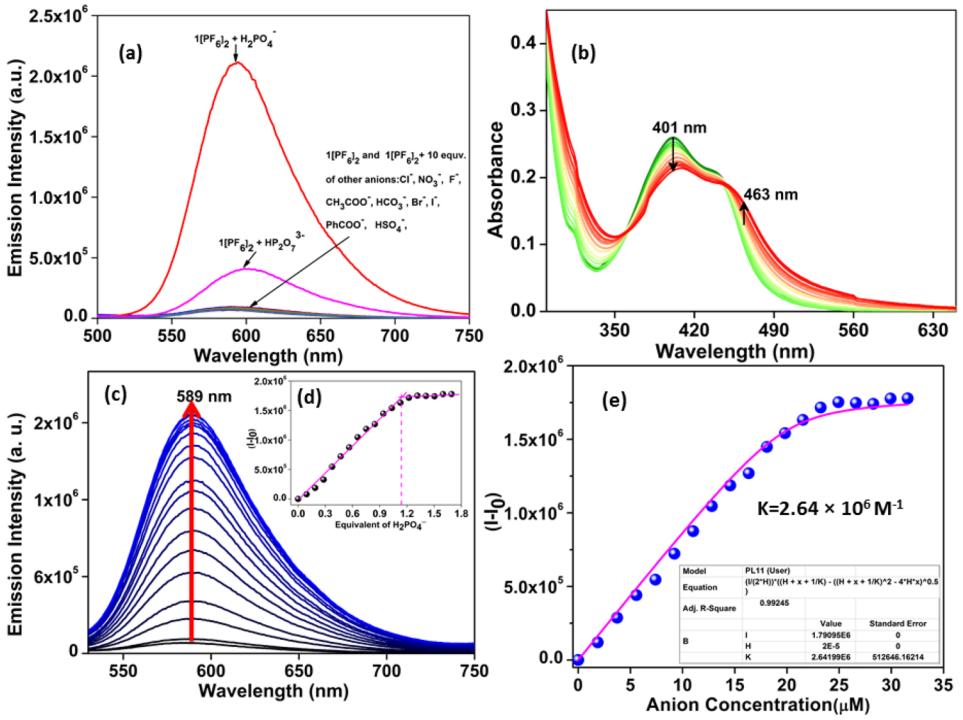

Figure 1. (a) Changes in the PL spectrum of $\mathbf{1}[\mathbf{PF_6}]_2$ upon addition of various anions (10 equiv). (b) UV titration of receptors $\mathbf{1}[\mathbf{PF_6}]_2$ with $H_2PO_4^-$. (c) PL titration of receptors $\mathbf{1}[\mathbf{PF_6}]_2$ with $H_2PO_4^-$ (Inset (d): anion equivalent plot). (e) Nonlinear fitting of PL titration data for $\mathbf{1}[\mathbf{PF_6}]_2$ with $H_2PO_4^-$.

and $\mathbf{9}[\mathbf{PF_6}]_2$ with various substituent groups. Thus, a pentafluorophenyl ring as the neighboring group substituent makes the maximum impact toward the phosphate-induced enhancement of emission intensity. To revalidate the influence of the pentafluorophenyl moiety, we have designed another complex, $\mathbf{7}[\mathbf{PF_6}]_2$, having bipyridine moiety in the central core unit instead of phenanthroline in $\mathbf{1}[\mathbf{PF_6}]_2$. Interestingly, $\mathbf{7}[\mathbf{PF_6}]_2$ also shows as high as ∼19-fold growth in ^{3}MLCT emission spectra with phosphate. The emission intensity amplification in all the complexes ($\mathbf{1}[\mathbf{PF_6}]_2$–$\mathbf{7}[\mathbf{PF_6}]_2$) with phosphates can be justified due to the probe backbone rigidification assisted by supramolecular self-assembly and hydrogen-bonding interactions, which are discussed below.

The binding constants of all the probes with $H_2PO_4^-$ were calculated to demonstrate the binding abilities and the selectivity of receptors toward the anion. The 1:1 (H:G) stoichiometric ratios of binding of receptors and phosphates were confirmed by the Job plot method using PL spectroscopy (Figure S60 in the Supporting Information). The association constants of $\mathbf{1}[\mathbf{PF_6}]_2$–$\mathbf{7}[\mathbf{PF_6}]_2$ with $H_2PO_4^-$ were calculated by a nonlinear fitting of the titration data in the 1:1 binding model, which show variation in the association constants ranging from 10^4 to 10^6 M^{-1} (Table 1 and Figure S61 in the Supporting Information). It is important to note that $\mathbf{1}[\mathbf{PF_6}]_2$ having a pentafluorophenyl substituent shows the highest association constant of 2.64×10^6 M^{-1} among all the probes, followed by $\mathbf{7}[\mathbf{PF_6}]_2$ with a value of 9.26×10^5 M^{-1}.

During titration, changes in emission intensity of all the probes with $H_2PO_4^-$ show a linear relationship with the $H_2PO_4^-$ concentration, which resulted in detection limits in the range of ∼0.013–0.067 μM for probes $\mathbf{1}[\mathbf{PF_6}]_2$–$\mathbf{7}[\mathbf{PF_6}]_2$, as calculated by specific quantitative analysis (Table S1 and Figure S62 in the Supporting Information). Notably, $\mathbf{1}[\mathbf{PF_6}]_2$ and $\mathbf{7}[\mathbf{PF_6}]$ also show the lowest detection limit of 0.013 and 0.018 μM, respectively, among all of the probes studied (Table S1 in the Supporting Information). All of these results confirm the superiority of the pentafluorophenyl-substituted triazole toward the selective sensing of $H_2PO_4^-$ through the highest fluorescence enhancement, association constants, and sensitivity.

The ^{1}H NMR experiment of all the receptors with $H_2PO_4^-$, in DMSO-d_6 at 298 K, shows a sharp singlet peak in the downfield region, which is recognized as a triazole proton peak. On the gradual addition of different anions, the acidic triazole proton of probes $\mathbf{1}[\mathbf{PF_6}]_2$–$\mathbf{6}[\mathbf{PF_6}]_2$ displays a steady downfield shift only with 1 equiv of $H_2PO_4^-$ (Figures S63 and S64 in the Supporting Information). However, competitive HSO_4^-, AcO^-, F^-, Br^-, Cl^-, NO_3^-, etc. anions do not display such visible ^{1}H NMR spectral changes with all of the probes. When higher amounts (2 equiv or more) of basic anions such as F^- and AcO^- are added, slight downfield shifts are noted for the triazole proton, signifying the requirement of a high analyte concentration of F^- and AcO^- for the interaction with a triazole proton. It is worth mentioning here that the protons of naphthalene, anthracene, and pyrene units do not show observable shifts upon complexation with anions (Figure S64b–d in the Supporting Information). This demonstrates that the interactions in all of the probes purely occur only between the triazole proton and phosphate through a hydrogen-bonding interaction. A Job plot analysis from the ^{1}H NMR experiment of $\mathbf{1}[\mathbf{PF_6}]_2$ with $H_2PO_4^-$ also shows a 1:1 (H:G) stoichiometric binding complex (Figure S65 in the Supporting Information).

The ^{31}P NMR spectra in DMSO-d_6 confirm $H_2PO_4^-$ binding with the probes, where PPh_3 is used as an external standard. When 1 equiv of $\mathbf{1}[\mathbf{PF_6}]_2$ and $\mathbf{7}[\mathbf{PF_6}]_2$ was added to free phosphate, the ^{31}P resonance at 2.98 ppm shifted upfield to 1.50 and 2.21 ppm, respectively, which may be due to an

https://doi.org/10.1021/acs.inorgchem.1c01084
Inorg. Chem. 2021, 60, 9084–9096

Table 2. Comparative Data of Diffusion Coefficients D (m^2 s^{-1}) Obtained from NMR and Dynamic Light Scattering Recorded for All Complexes ($1[PF_6]_2$–$7[PF_6]_2$) and with $H_2PO_4^-$ in DMSO-d_6 at 298 K

entry		^{1}H-DOSY NMR			dynamic light scattering (DLS)	
host	guest	diffusion coefficient D (m^2/S)	calcd radius (nm)[a]	sphere volume ratio (B/A)	size d (nm)	sphere volume ratio (B/A)
$1[PF_6]_2$	(A) none	7.188×10^{-10}	0.1546	82.5	143	92.8
	(B) $H_2PO_4^-$	1.659×10^{-10}	0.6700		647	
$2[PF_6]_2$	(A) none	7.365×10^{-10}	0.1509	14.3	152	15.9
	(B) $H_2PO_4^-$	3.087×10^{-10}	0.3600		383	
$3[PF_6]_2$	(A) none	3.601×10^{-10}	0.3087	10.2	163	10.8
	(B) $H_2PO_4^-$	1.684×10^{-10}	0.6600		361	
$4[PF_6]_2$	(A) none	8.230×10^{-10}	0.1350	16.7	196	18.4
	(B) $H_2PO_4^-$	3.269×10^{-10}	0.3400		518	
$5[PF_6]_2$	(A) none	7.953×10^{-10}	0.1398	20.6	130	23.8
	(B) $H_2PO_4^-$	2.925×10^{-10}	0.3800		374	
$6[PF_6]_2$	(A) none	8.076×10^{-10}	0.1376	11.8	135	14
	(B) $H_2PO_4^-$	3.585×10^{-10}	0.3100		326	
$7[PF_6]_2$	(A) none	1.136×10^{-9}	0.0978	138.7	141	143
	(B) $H_2PO_4^-$	2.179×10^{-10}	0.5100		739	

[a]Using the Stokes–Einstein equation.

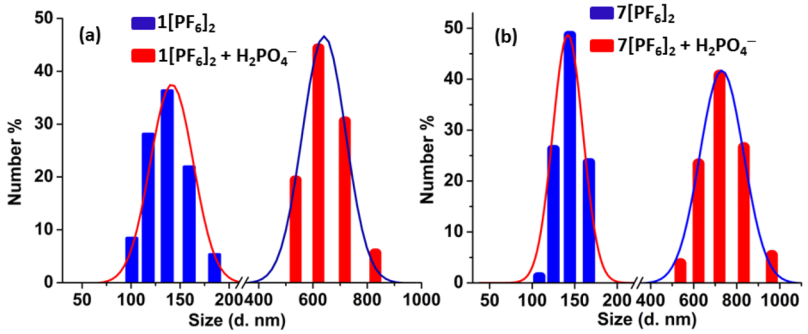

Figure 2. Comparative DLS study of (a) $1[PF_6]_2$ and (b) $7[PF_6]_2$ in the absence and presence of phosphates.

anion–π interaction of the pentafluorophenyl group and phosphate anions (Figure S66 in the Supporting Information). However, with the addition of receptors $2[PF_6]_2$ and $3[PF_6]_2$ to $TBAH_2PO_4$, the ^{31}P peak shifted weakly to the downfield region. The shifts (downfield or upfield) of the ^{31}P peaks indicate an interaction of the phosphate oxygen atoms and probes, as previously reported in the literature.[24]

To understand the superiority of the probes $1[PF_6]_2$ and $7[PF_6]_2$ in terms of enhancement in the ^{3}MLCT emission spectra, binding constant, and detection limit, ^{19}F NMR studies were performed. Two sharp peaks at 71.2 and 73.3 ppm in ^{19}F NMR spectra were recognized as a fluorine of PF_6^- in DMSO-d_6 at 298 K. The peaks at −143.6, −154.3, and −163.6 ppm were identified as *o*-, *p*-, and *m*-fluorine, respectively, of the pendant pentafluorophenyl group of probes $1[PF_6]_2$ and $7[PF_6]_2$ (Figure S67 in the Supporting Information). These distinctive chemical shifts provide a multidimensional spectroscopic signature without complexity from overlapping ^{19}F NMR signals. Binding of $H_2PO_4^-$ to the receptors $1[PF_6]_2$ and $7[PF_6]_2$ yield upfield shifts (−144.1, −155.2, and −164.8 ppm for $1[PF_6]_2$ and −145.1, − 155.4, and −164.4 ppm for $7[PF_6]_2$; *o*-, *p*-, and *m*-fluorine, respectively) in the ^{19}F NMR of the pentafluorophenyl group. The upfield shift of ^{19}F peaks of the pendant pentafluorophenyl group of $1[PF_6]_2$ and $7[PF_6]_2$ indicates a phosphate interaction with the electron-deficient pentafluorophenyl group in solution, which could be due to an anion–π interaction. This eventually helps in the phosphate-assisted extended aggregation of $1[PF_6]_2$ and $7[PF_6]_2$ probes and makes them efficient sensors in comparison to the others.

Solution-State Aggregation as Well as Macroscopic Morphological Analysis. To establish the aggregation-induced sensing property of this generation of probes, ^{1}H-DOSY NMR experiments of all of the complexes with phosphates (e.g., $H_2PO_4^-$) were performed to understand the adducts formed between the probes and phosphate in DMSO-d_6 at 298 K (Figure S68 in the Supporting Information). It has been found that the diffusion coefficients of all the free probes are reduced considerably in the presence of 1 equiv of $H_2PO_4^-$ (Table 2). The maximum decrease in the diffusion coefficient value is observed for phosphate adducts of the probes $1[PF_6]_2$ and $7[PF_6]_2$. The diffusion coefficient value decreased from 7.188×10^{-10} to 1.659×10^{-10} m^2/S and from 1.136×10^{-9} to 2.179×10^{-10} m^2/S for the phosphate adducts of $1[PF_6]_2$ and $7[PF_6]_2$, respectively, which may be due to the formation of larger aggregated species in solution in comparison to the other probes. Thus, it is clearly evident that phosphate adduct complexes in solution are considerably greater in size, dissimilar from free anion complexes. Zapata et al. has recently reported such supramolecular polymeric aggregates in solution where the role of cooperative action of noncommon antielectrostatic anion–anion and halogen-bonding interactions has been indicated.[51] Thus, the supramolecular aggregated structure of probes in solution here could be through hydrogen bonding and uncommon antielectrostatic anion–anion interactions as well. It may also be noted that

https://doi.org/10.1021/acs.inorgchem.1c01084
Inorg. Chem. 2021, 60, 9084–9096

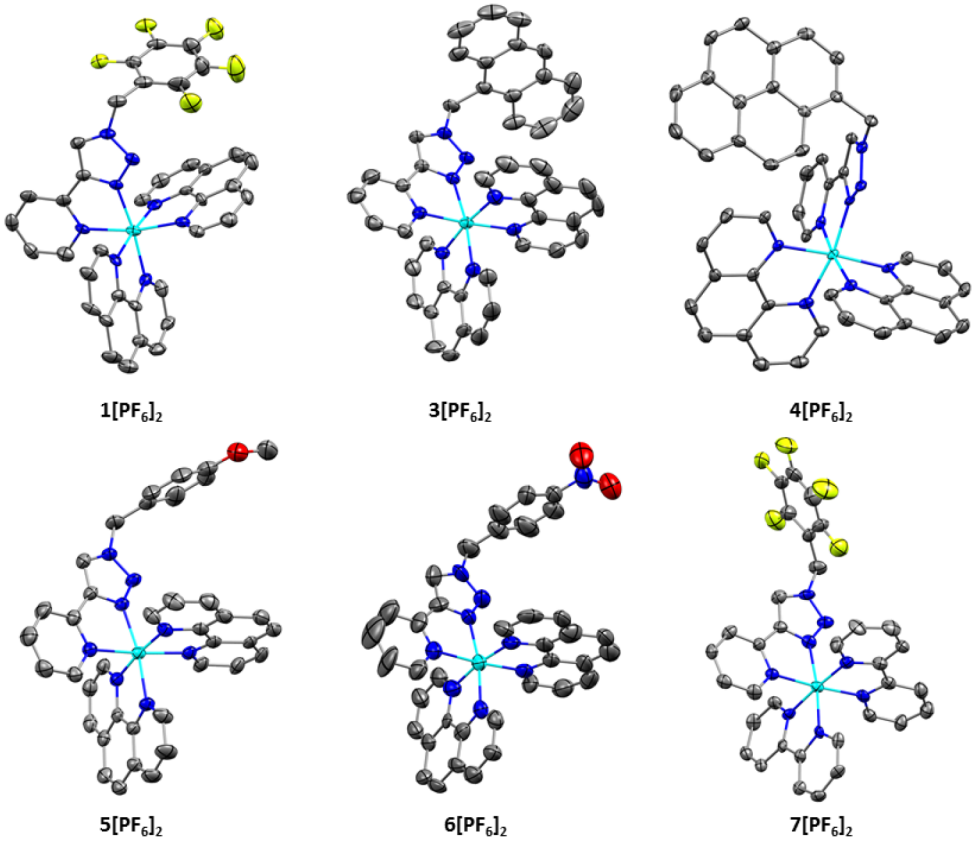

Figure 3. Single-crystal structures of $\mathbf{1}[PF_6]_2$ and $\mathbf{3}[PF_6]_2$–$\mathbf{7}[PF_6]_2$. Counteranions, solvent molecules, and all H atoms (except triazole H) are omitted for clarity. Color code: C, gray; Ru, cyan; N, blue; O, red; H, white; F, green.

such supramolecular aggregates could be assisted by an anion–π interaction (for $\mathbf{1}[PF_6]_2$ and $\mathbf{7}[PF_6]_2$) and a π–π stacking interaction (for $\mathbf{3}[PF_6]_2$ and $\mathbf{4}[PF_6]_2$) as observed in literature reports.[52]

The formation of higher-order aggregated species in solution can also be verified by carrying out DLS experiments of all the receptors $\mathbf{1}[PF_6]_2$–$\mathbf{7}[PF_6]_2$) in the absence as well as in the presence of $H_2PO_4^-$ in DMSO at 298 K (Figure 2 and Figure S69 in the Supporting Information). Interestingly, the initial hydrodynamic diameters of all the free receptors increase significantly in the presence of $H_2PO_4^-$, which is due to the formation of supramolecular aggregates of phosphate adducts. All of the data are given in Table 2. Larger hydrodynamic radii of 647 and 739 nm are found for adducts of phosphate and $\mathbf{1}[PF_6]_2$ and $\mathbf{7}[PF_6]_2$, respectively. These data reveal the formation of higher-order supramolecular self-assembled structures in the solution. Representative data of the formation of higher-order supramolecular aggregates in the solution are shown in Figure 2. Further, a transmission electron microscopy (TEM) study was performed to support the preliminary experimental observation of the formation of anion-assisted supramolecular polymeric aggregates. Spherical types of micellar/vesicular type morphological structures resulted in the cases of the free receptors $\mathbf{1}[PF_6]_2$, $\mathbf{4}[PF_6]_2$, and $\mathbf{5}[PF_6]_2$ in the TEM study. On further additions of 1 equiv of phosphate to the receptors, the spherical micellar/vesicular structures are transformed to supramolecular aggregates (Figures S70 and S71 in the Supporting Information). Thus, the morphological transformation upon addition of phosphate suggests the formation in solution of supramolecular aggregates, which may also be assisted by anion–π or π–π stacking as reported earlier with different anion-supported assemblies.[50,53]

It should be noted that the aggregates stop growing at a particular size without the availability of capping agents. Indeed, different types of van der Waal forces of attractions help the nucleation process for the formation of aggregates. However, a competition starts between the short-range forces operating over small distances and the inertial forces which operate when the particles become larger. This might eventually help to overcome the attractive van der Waals forces toward stopping of the growth of aggregates at a particular size.

Single-Crystal Structures of the Probes and Phosphate Complexes of the Probes. Crystals suitable for single-crystal X-ray diffraction structural analyses of six probes, $\mathbf{1}[PF_6]_2$ and $\mathbf{3}[PF_6]_2$–$\mathbf{7}[PF_6]_2$ were obtained from a dichloromethane and dimethylformamide/methanol (1/1) solution mixture of complexes via a slow evaporation method. $\mathbf{1}[PF_6]_2$, $\mathbf{4}[PF_6]_2$, and $\mathbf{6}[PF_6]_2$ crystallize in a triclinic crystal system with $P\bar{1}$ space group, whereas $\mathbf{3}[PF_6]_2$, $\mathbf{5}[PF_6]_2$, and $\mathbf{7}[PF_6]_2$ crystallize in a monoclinic crystal system with $P2_1/n$, $C2/c$, and $P2_1/c$ space groups, respectively. An exploration of the crystal structures of all these probes reveals that the Ru(II) center adopts a distorted-octahedral geometry in $\mathbf{1}^{2+}$ and $\mathbf{3}^{2+}$–$\mathbf{7}^{2+}$, where four sites are occupied by four coordinating N centers of two phenanthrolines (bipyridine rings for $\mathbf{7}^{2+}$) and the other two coordination sites of the distorted octahedra are occupied by two N atoms of pyridine triazole (Figure 3). The detailed crystallographic information along with all bond lengths and

https://doi.org/10.1021/acs.inorgchem.1c01084
Inorg. Chem. 2021, 60, 9084–9096

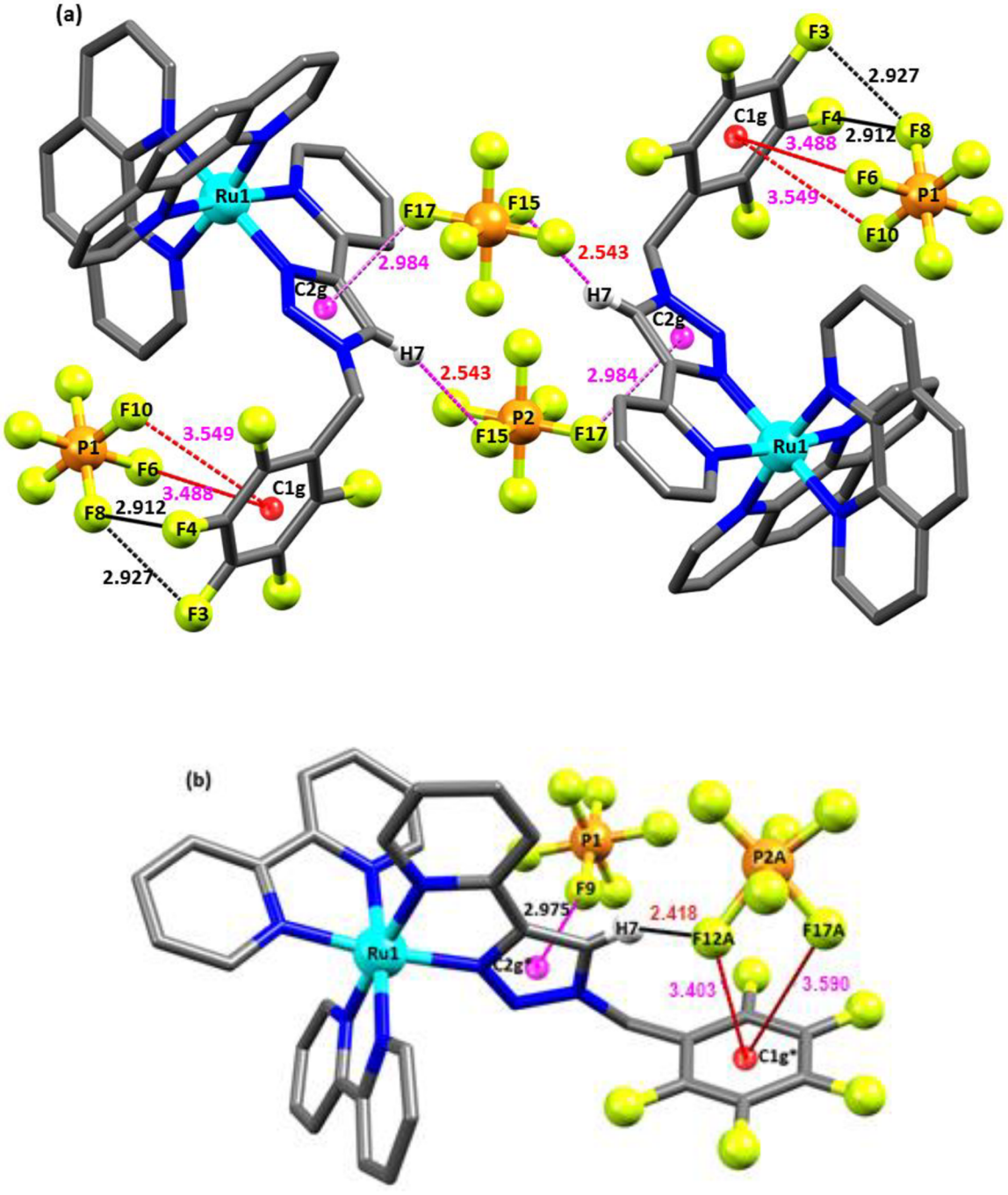

Figure 4. Crystal structures of (a) $\mathbf{1}[\mathbf{PF_6}]_2$ and (b) $\mathbf{7}[\mathbf{PF_6}]_2$ showing C−H···F and F···F interactions and showing combined C−H···F and an anion F−π interaction. Color code: C, gray; Ru, cyan; N, blue; H, white; F, yellowish green; P, orange yellow.

angles are provided in Tables S2−S4 in the Supporting Information, which is well-matched with the literature reports.[27,47,50] Packing diagrams of all the crystals reveal a noncovalent 3D network through C−H···F contacts among triazole C−H and F atom of $[PF_6]^-$ (Figures S72−S77 in the Supporting Information). A further exploration of the crystal structures of $\mathbf{1}[\mathbf{PF_6}]_2$ and $\mathbf{7}[\mathbf{PF_6}]_2$ shows that the probes are associated with the $[PF_6]^-$ via a C−H···F hydrogen-bonding contact with the triazole pyridine. The stronger interaction is found between the hydrogen atom of the triazole pyridine group (C−H7) and the fluorine atom (F15) of $[PF_6]^-$ with an H···F distance of 2.543 Å in the case of $\mathbf{1}[\mathbf{PF_6}]_2$, whereas that between the hydrogen atom of the triazole pyridine group (C−H7) and fluorine atom (F12A) of $[PF_6]^-$ has an H···F distance of 2.418 Å in $\mathbf{7}[\mathbf{PF_6}]_2$. In addition, the fluorine atoms of $[PF_6]^-$ have anion···π interactions with C_6F_5 and triazole units with the distances C1g···F6 (3.488 Å), C1g···F10 (3.549 Å), and C2g···F17 (2.984 Å) for $\mathbf{1}[\mathbf{PF_6}]_2$ and C1g*···F12A (3.403 Å), C1g*···F17A (3.590 Å), and C2g*···F9 (2.975 Å) for $\mathbf{7}[\mathbf{PF_6}]_2$, where C1g/C1g* and C2g/C2g* are the centroids of the C_6F_5 and triazole moiety of $\mathbf{1}[\mathbf{PF_6}]_2$ and $\mathbf{7}[\mathbf{PF_6}]_2$, respectively (Figure 4 and Figures S72 and S77 in the Supporting Information).[54−56] Also, a π−π stacking interaction is observed between pyrene units for the complex $\mathbf{4}[\mathbf{PF_6}]_2$ in the solid state (Figure S74 in the Supporting Information).

https://doi.org/10.1021/acs.inorgchem.1c01084
Inorg. Chem. 2021, 60, 9084−9096

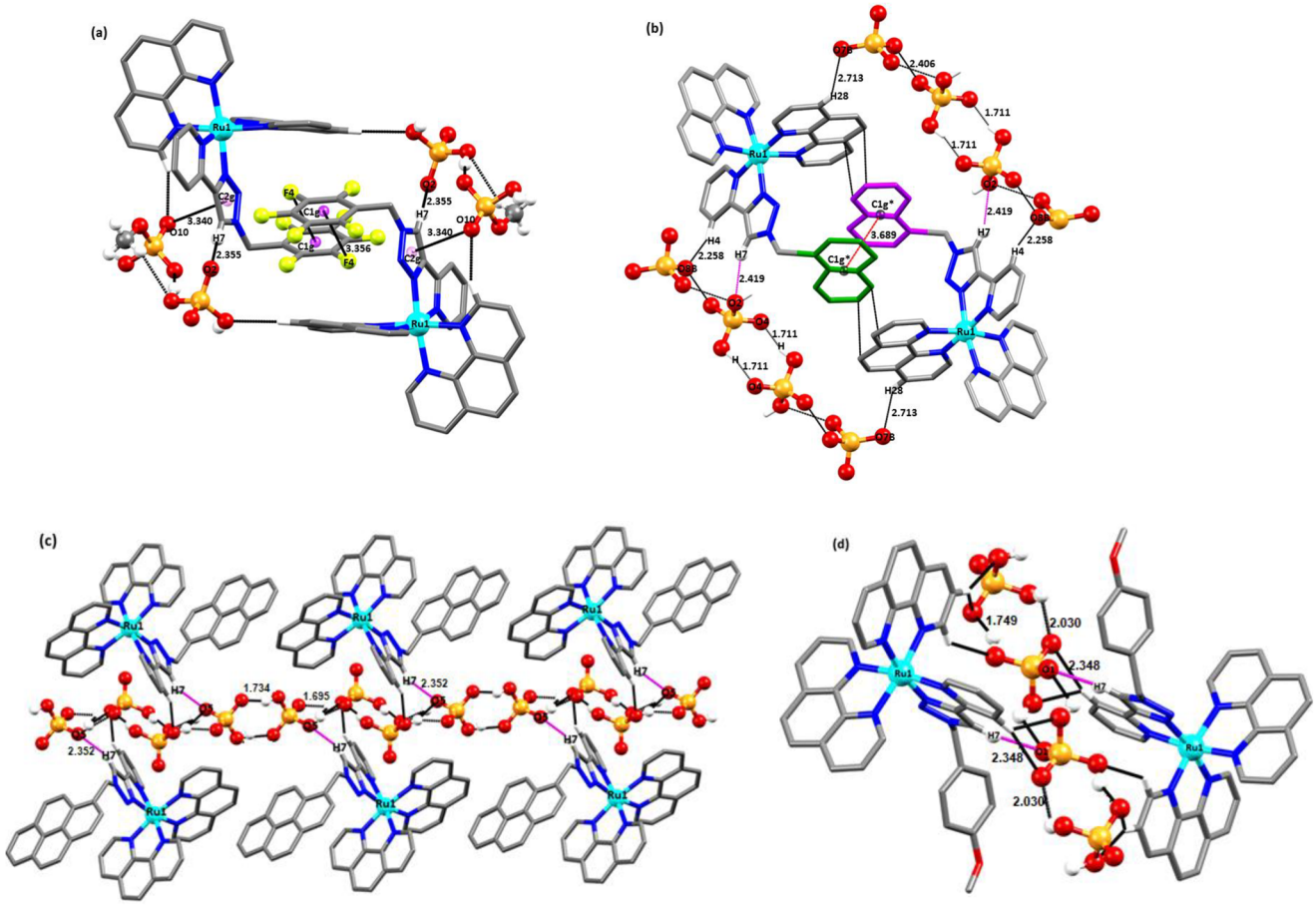

Figure 5. (a) Single-crystal X-ray structure of $\mathbf{1}[\mathbf{H_2PO_4}]_2$ where a phosphate chain is propagated infinitely via triazole phosphate (C−H···O) hydrogen bonding as well as an anion−π interaction between fluorine and the C_6F_5 unit (b) Single-crystal X-ray structure of $\mathbf{2}[\mathbf{H_2PO_4}]_2$ propagated by combined hydrogen bonding and π−π stacking interactions between naphthalene moieties. (c, d) Single-crystal X-ray structures of $\mathbf{4}[\mathbf{H_2PO_4}]_2$ and $\mathbf{5}[\mathbf{H_2PO_4}]_2$ in which phosphate binds with triazole through C−H···O and hydrogen-bonding interactions. Distances are shown in Å, and all of the H atoms (except triazole C−H) are removed for clarity. Color codes: Ru, cyan; C, gray, green, pink; N, blue; H, white; F, green; P, orange-yellow; O, red.

To study the phosphate binding of bis-heteroleptic Ru(II) complexes of triazole probes in the solid state, we have crystallized the receptors in the presence of $H_2PO_4^-$. Crystals of $H_2PO_4^-$ adducts of $\mathbf{1}^{2+}$, $\mathbf{2}^{2+}$, $\mathbf{4}^{2+}$, and $\mathbf{5}^{2+}$ suitable for single-crystal X-ray diffraction studies are achieved by slow diffusion of diethyl ether in DMF/methanol solution of probes $\mathbf{1}[\mathbf{PF_6}]_2$, $\mathbf{2}[\mathbf{PF_6}]_2$, $\mathbf{4}[\mathbf{PF_6}]_2$, and $\mathbf{5}[\mathbf{PF_6}]_2$, respectively. The crystal parameters, data collection, and refinement details of the crystals of $\mathbf{1}[\mathbf{H_2PO_4}]_2$, $\mathbf{2}[\mathbf{H_2PO_4}]_2$, $\mathbf{4}[\mathbf{H_2PO_4}]_2$, and $\mathbf{5}$-$[\mathbf{H_2PO_4}]_2$ are summarized in Tables S2 and S3 in the Supporting Information. All of these complexes are crystallized in a triclinic crystal system with the $P\bar{1}$ space group. The Ru(II) metal centers of $\mathbf{1}^{2+}$, $\mathbf{2}^{2+}$, $\mathbf{4}^{2+}$, and $\mathbf{5}^{2+}$ units in phosphate complexes display a distorted-octahedral geometry wherein four coordination sites of the Ru(II) center are engaged by two phenanthroline moieties, and the other two coordination sites are coordinated by different pyridine triazole units as observed in the cases of PF_6^- salts of the respective the bis-heteroleptic Ru(II)-complexes.

The asymmetric unit of the complex $\mathbf{1}[\mathbf{H_2PO_4}]_2$ is found to be comprised of one $\mathbf{1}^{2+}$ unit, two occluded phosphate anions, and one occluded phosphate methyl ester formed during the course of the synthesis of the complex, which are all fully occupied and located on general positions. A few smeared electron densities of disordered solvent molecules could not be accurately modeled and hence were squeezed out. The squeeze calculation reveals that the electron densities are equivalent to two DMF molecules. The occluded phosphate anions are extensively hydrogen bonded among themselves by the usual extended dimeric phosphate···phosphate hydrogen bonding interactions (O···H−O), which are in the range between 1.625 and 2.630 Å along with an extra stabilization by hydrogen bonding with the occluded phosphate methyl ester formed during the synthesis of the complex. Thus, phosphate anions form a 2D hydrogen-bonded network by the cumulative hydrogen bonding described above, which provides an extra stabilization of the phosphate anions within the crystal lattice. The packing of the complex offers a continuous channel where the phosphates and the loosely bound disordered solvent molecules are located within the channel as well as within the interstitial space between the arrays of the complex sustained by H-bonding interactions (Figure S78 in the Supporting Information). Interestingly, the triazole C−H of $\mathbf{1}^{2+}$ formed a strong and directional hydrogen-bonding contact with $H_2PO_4^-$, having a bonding distance (O2···H7) of 2.355 Å and an angle ($\angle$C−H7···O2) of 160.15°. Anion···π interactions are also found between the F4 atom and the electron-deficient C_6F_5 ring of $\mathbf{1}[\mathbf{H_2PO_4}]_2$, as well as the oxygen atom of $H_2PO_4^-$

https://doi.org/10.1021/acs.inorgchem.1c01084
Inorg. Chem. 2021, 60, 9084−9096

anion and triazole moiety with the shortest distance C1g···F4 being 3.356 Å and that of C2g···O10 3.340 Å (Figure 5a), as observed in previously reported systems.[27,47,50,56,57] All of these interactions probably assist the probe rigidification effectively.

In the case of the complex $\mathbf{2}[\mathbf{H_2PO_4}]_2$, one of the two phosphates (refined SOF = 0.50944:0.49056) and the naphthalene moiety (refined SOF = 0.55163:0.44837) of the ligand are found to be disordered over two positions. Packing of the complex along the *ab* plane provides a continuous channel along the *b* axis wherein the phosphates are located and are sustained by dimeric phosphate···phosphate hydrogen-bonding interactions (Figure S79b in the Supporting Information). Furthermore, the phosphates are found to show a weak anion···π interaction (4.08 Å) with the coordinated phenanthroline moieties. Importantly, strong hydrogen bonding between the triazole C−H and the oxygen atom of $H_2PO_4^-$ is found with an O2···H7 distance of 2.414 Å along with a $\pi-\pi$ stacking interaction distance between the centroid and the centroid (C1g*···C1g*) interligand pendant naphthalene units of 3.689 Å (C1g*···C1g*) in $\mathbf{2}[\mathbf{H_2PO_4}]_2$ (Figure 5b and Figure S79a in the Supporting Information).[58] In the case of the complex $\mathbf{4}[\mathbf{H_2PO_4}]_2$ one $\mathbf{4}^{2+}$ and two occluded phosphates are all fully occupied and located on available positions in the asymmetric unit of the complex. Furthermore, smeared electron densities of disordered solvent molecules could not be accurately modeled and consequently were squeezed out. A squeeze calculation reveals the presence of three disordered methanol molecules in the asymmetric unit. One of the phosphate anions was found to be disordered over two positions (refined SOF = 0.81755:0.18245). Packing of the complex generated a void channel wherein the phosphates were located and sustained by dimeric 1D phosphate···phosphate hydrogen bonding (Figure 5c). In the case of the complex $\mathbf{5}[\mathbf{H_2PO_4}]_2$ one $\mathbf{5}^{2+}$ and two occluded phosphate anions are all fully occupied and located in general positions (Figure 5d). The methoxybenzene moiety of the ligand is found to be disordered over two positions (refined SOF = 0.52333:0.47667). The phosphates are found to show fragile anion···π interactions (4.26 Å) with the disordered methoxybenzene moieties of the ligand. Packing of the complex generated a void channel wherein the phosphates were located and sustained by dimeric phosphate···phosphate hydrogen bonding. Thus, overall strong extensively hydrogen bonded interactions between triazole and phosphate oxygen atoms, as well as between the occluded phosphate anions and solvent molecules, occur in all four phosphate complexes, $\mathbf{1}[\mathbf{H_2PO_4}]_2$, $\mathbf{2}[\mathbf{H_2PO_4}]_2$, $\mathbf{4}[\mathbf{H_2PO_4}]_2$, and $\mathbf{5}[\mathbf{H_2PO_4}]_2$, to construct the polymeric assembly in the solid state (Figures S78 and S80 in the Supporting Information).

CONCLUSION

Studies on a series of nine bis-heteroleptic Ru(II) receptors having a pyridine triazole moiety as an anion-binding unit with various substituents on the triazole have established this series of metal complexes as selective probes for dihydrogen phosphate. Further, we have determined that enhancement-based selective sensing is via the selective formation of phosphate-supported extensive self-assembled structures. It has also been found that the change in the aromaticity or electronic parameter of the substituents on the probes $\mathbf{2}[\mathbf{PF_6}]_2$−$\mathbf{6}[\mathbf{PF_6}]_2$, $\mathbf{8}[\mathbf{PF_6}]_2$, and $\mathbf{9}[\mathbf{PF_6}]_2$ moderately influences the effective sensing of $H_2PO_4^-$. Significantly, the probes with a pentafluorophenyl moiety, $\mathbf{1}[\mathbf{PF_6}]_2$ and $\mathbf{7}[\mathbf{PF_6}]_2$, are superior to all other probes in the series in terms of a large amplification of emission intensity, an enhanced binding constant, and a lower detection limit. Such a distinction of the pentafluorophenyl substituent in $\mathbf{1}[\mathbf{PF_6}]_2$ and $\mathbf{7}[\mathbf{PF_6}]_2$ has been correlated with the formation of larger polymeric aggregates of the probes with $H_2PO_4^-$ in solution, which is evident from the DOSY and DLS studies, which eventually rigidified the system more effectively. We envisaged that such an understanding of the phosphate sensing pathways in Ru(II) polypyridyl based receptors might be advantageous in planning better sensors for various anions.

EXPERIMENTAL SECTION

Materials. All of the reactions were performed under an inert atmospheric environment, followed by an ambient conditions workup. Acetonitrile was refluxed over calcium hydride and was collected afore use. $RuCl_3{\cdot}xH_2O$, 1,10-phenanthroline, deuterated solvents, tetrabutylammonium salts of the anions HSO_4^-, NO_3^-, $CH_3CO_2^-$, HCO_3^-, $C_6H_5CO_2^-$, I^-, Br^-, Cl^-, F^-, $H_2PO_4^-$, and $HP_2O_7^{3-}$, zinc perchlorate, and potassium hexafluorophosphate were purchased from Sigma-Aldrich and were used as received. Ethanol was procured from Spectrochem Private Limited. All physical studies were carried out by using spectroscopy-grade solvents. Distilled and well-degassed ethanol/water mixtures (2/1 v/v and 3/4 v/v respectively) were used for the synthesis of probes.

Methods. A Shimadzu FTIR-8400S infrared spectrophotometer was used for recording FTIR. Elemental analysis was performed on a PerkinElmer 2500 series II elemental analyzer (PerkinElmer, USA). HRMS analysis was done on a QToF-Micro YA 263 mass spectrometer in ESI (+ve) mode. A Bruker FT-NMR DPX 500/400/300 MHz NMR spectrometer was used to record all types of NMR data. The chemical shift (δ) values for ^{1}H, ^{13}C, ^{31}P, and ^{19}F NMR are reported in parts per million (ppm), and the peak positions were calibrated using TMS as an internal standard. All ^{31}P NMR experiments were carried out in the presence of triphenylphosphine (used as an external standard). A PerkinElmer Lambda 900 UV/vis/NIR spectrometer (with 1 cm path length of the quartz cuvette) was used to record absorption spectra, whereas a FluoroMax-3 spectrophotometer (Horiba-JobinYvon) was used to record emission spectra.

Caution! Perchlorate salts and organic azide(I) are potentially explosive under certain conditions. These materials should be used with proper precaution. However, we did not face any difficulty in handling these materials.

Calculation of Association Constants. Associations between probes $\mathbf{1}[\mathbf{PF_6}]_2$−$\mathbf{7}[\mathbf{PF_6}]_2$ and $H_2PO_4^-$ were calculated using PL titration data. The emission spectra of probes increased progressively due to the binding of the phosphate anion to the receptor. The corresponding association constant (K_a) was determined by a nonlinear fitting of curves that was obtained by plotting the changes in emission (ΔI) at a fixed wavelength against the concentration of the anions added. All of the PL titration data were fitted to eq 1 for 1:1 binding

$$\Delta I = \left(\frac{I}{2H}\right)\left\{\left(H + X + \frac{1}{K_a}\right) - \sqrt{\left(H + X + \frac{1}{K_a}\right)^2 + 4HX}\right\} \quad (1)$$

where I = emission intensity of the probes upon each addition of the $H_2PO_4^-$ anion, $\Delta I = I - I_0$, H = probe concentration, and X = $H_2PO_4^-$ concentration.[59,60]

Calculation of Detection Limit. The detection limit (DL) was calculated using eq 2

$$\mathrm{DL} = \frac{3\mathrm{SD}}{\mathrm{slope}} \quad (2)$$

https://doi.org/10.1021/acs.inorgchem.1c01084
Inorg. Chem. 2021, 60, 9084−9096

where SD corresponds to the standard deviation of the value of luminescence intensity of the blank sample, measured for 10 consecutive scans. The slope was calculated from the linear fit plot of the change in emission intensity vs the concentration of the anion.

X-ray Crystallographic Refinement Details. The crystallographic details of the probes are given in Table S2 in the Supporting Information. A Bruker SMART APEX diffractometer having Mo Kα (λ = 0.7107 Å) radiation was used to collect intensity data of the crystal, and the instrument was equipped with a CCD area detector. SAINT[61] software was used for the integration and reduction of data. SADABS[62] was applied for an empirical absorption correction to the collected reflections. SHELXTL[63] and SHELXL-2014[64] were utilized to solve the structure and refined on F^2 by the full-matrix least-squares technique, respectively. Graphics were created with the help of PLATON-97[65] and MERCURY 3.7.[66] The PLATON/SQUEEZE program was applied to account for some disordered solvent molecules that we have not been able to assign properly. The CCDC file numbers of the crystal structures (2048424−2048433) contains the crystallographic data for this paper.

Synthesis. The ligands L1−L6 were synthesized and then were used in synthesizing complexes (details of ligand synthesis are given in the experimental section in the Supporting Information).

General Synthetic Procedure of the Complexes. *cis*-[Ru(phen)$_2$Cl$_2$] and *cis*-[Ru(bpy)$_2$Cl$_2$] were synthesized by a reported procedure.[67] Further, they were used for the synthesis of complexes. L (0.28 mmol) and *cis*-[Ru(phen)$_2$C$_{l2}$]/*cis*-[Ru(phen)$_2$C$_{l2}$] (0.28 mmol) were placed in a 100 mL three-neck round-bottom (RB) flask. The flask was degassed and purged with argon several times. After that 40 mL of a well-degassed ethanol/water mixture (2/1 v/v and 3/4 v/v, respectively) was placed in the flask through a septum under an argon atmosphere. The mixture was heated to reflux under an argon atmosphere for 24 h. After evaporation of ethanol, the reaction mixture was cooled to room temperature. Then a saturated solution of KPF_6 (450 mg) was added to the reaction mixture, and this mixture was stirred for up to 30 min to complete the precipitation. The orange-red or yellow-orange precipitate was dissolved in dichloromethane. The organic phase was washed with brine solution followed by distilled water. The organic layer was evaporated to obtain a crude yellow-orange solid, which was further purified through column chromatography using 60−120 mesh silica gel and $CH_3CN/H_2O/KNO_3$ (90/9.5/0.5) as eluent. During column chromatography in the dark, the orange band was collected as the nitrate salt of the complex. The collected portion was concentrated and treated with excess KPF_6 salt dissolved in water. After addition, an orange-red/yellow-orange precipitate was formed, which was filtered, washed with water, and dried under vacuum to give the desired crystalline solid product.

***1*[PF$_6$]$_2$.** Anal. Calcd for $C_{38}H_{23}N_8RuP_2F_{17}$ (M_w = 1078.0293) C, 42.35; H, 2.15; N, 10.40. Found: C, 42.33; H, 2.12; N, 10.39. FTIR in KBr disk (ν/cm^{-1}): 3421, 1660, 1512, 1429, 1357, 11128, 1026, 842, 720. ESI-MS: for $[C_{38}H_{23}N_8RuPF_{11}]^+$, calcd m/z 933.0646, found m/z 933.0646; for $[C_{38}H_{23}N_8RuPF_5]^{2+}$, calcd m/z 394.0499, found m/z 394.0469; ^{1}H NMR (400 MHz, acetone-d_6): δ 9.24 (s, 1H), 8.83 (d, J = 8.4 Hz, 2H), 8.75 (d, J = 9.2 Hz, 1H), 8.70 (d, J = 9.2 Hz, 1H), 8.61 (d, J = 5.2 Hz, 1H), 8.58 (d, J = 5.2 Hz, 1H), 8.46 (d, J = 5.2 Hz, 1H), 8.40−8.33 (m, 5H), 8.22 (d, J = 6.4 Hz, 1H), 8.08 (t, J = 6.4 Hz, 1H), 7.99−7.92 (m, 2H), 7.87 (d, J = 5.6 Hz, 1H), 7.78 (dd, J = 8.2, 5.2 Hz, 1H), 7.69 (dd, J = 8, 5.2 Hz, 1H), 7.31 (t, J = 7.2 Hz, 1H), 5.82 (s, 2H) ppm. ^{13}C NMR (100 MHz, acetone-d_6): δ 154.2, 154.18, 154.16, 153.9, 153.1, 152.0, 149.4, 149.0, 148.9, 148.8, 139.2, 137.9, 137.86, 137.82, 137.4, 132.0, 131.9, 131.6, 131.3, 129.0, 128.8, 128.6, 127.2, 127.1, 127.06, 127.01, 126.3, 123.7, 43.8 ppm.

***2*[PF$_6$]$_2$.** Anal. Calcd for $C_{42}H_{30}N_8RuP_2F_{12}$ (M_w = 1038.0921) C, 48.61; H, 2.91; N, 10.80. Found: C, 48.60; H, 2.89; N, 10.79. FTIR in KBr disk (ν/cm^{-1}): 1623, 1512, 1429, 1027, 840, 721. ESI-MS: for $[C_{42}H_{30}N_8RuPF_6]^+$, calcd m/z 893.1273, found m/z 893.1274; for $[C_{42}H_{30}N_8Ru]^{2+}$, calcd m/z 374.0813, found m/z 374.0812. ^{1}H NMR (400 MHz, acetone-d_6): δ 9.07 (s, 1H), 8.85 (d, J = 8.4 Hz, 2H), 8.76 (d, J = 7.6 Hz, 1H), 8.72 (d, J = 8 Hz, 1H), 8.55 (t, d, J = 4 Hz, 2H), 8.47 (d, J = 5.2 Hz, 1H), 8.44−8.37 (m, 4H), 8.30 (d, J = 8 Hz, 1H), 8.25 (d, J = 5.2 Hz, 1H), 8.02 (t, J = 8 Hz, 1H), 7.98−7.91 (m, 4H), 7.85 (d, J = 5.6 Hz, 1H), 7.79 (dd, J = 8.2, 5.6 Hz, 1H) 7.72 (dd J = 8, 5.2 Hz, 1H), 7.61 (d, J = 8.4 Hz, 1H), 7.53 (t, J = 8 Hz, 1H), 7.46 (d, J = 5.2 Hz, 2H) 7.30−7.22 (m, 2H), 6.10 (q, J = 6.8 Hz, 2H) ppm. ^{13}C NMR (100 MHz, acetone-d_6): δ 154.2, 154.1, 154.0, 153.7, 153.1, 152.2, 149.4, 149.2, 149.05, 149.01, 148.9, 139.1, 137.8, 137.7, 137.5, 134.8, 132.02, 132.01, 131.7, 131.6, 131.0, 130.2, 129.8, 129.3, 129.1, 129.07, 129.02, 128.7, 127.9, 127.7, 127.1, 127.09, 127.03, 126.8, 126.4, 126.3, 123.6, 123.2, 55.6 ppm.

***3*[PF$_6$]$_2$.** Anal. Calcd for $C_{46}H_{32}N_8RuP_2F_{12}$ (M_w = 1088.1077): C, 50.79; H, 2.97; N, 10.30. Found: C, 50.78; H, 2.95; N, 10.27. FTIR in KBr disk (ν/cm^{-1}): 3434, 2923, 1724, 1548, 1427, 1122, 840, 723. ESI-MS: for $[C_{46}H_{32}N_8RuPF_6]^+$, calcd m/z 943.1430, found m/z 943.1432. ^{1}H NMR (500 MHz, acetone-d_6): δ 8.91 (s, 1H), 8.84 (d, J = 6.8 Hz, 1H), 8.78−8.74 (m, 2H), 8.72−8.69 (m, 2H), 8.50 (d, J = 4.6 Hz, 2H), 8.47 (d, J = 4.6 Hz, 1H), 8.42−8.36 (m, 5H), 8.21 (t, J = 4.8 Hz, 2H), 8.16 (dd, J = 6.8, 2.8 Hz, 4H), 7.96−7.94 (m, 1H), 7.93−7.89 (m, 1H), 7.85 (dd, J = 6.4, 4 Hz, 1H), 7.81 (d, J = 4.4 Hz, 1H), 7.78 (dd, J = 6.6, 4.4 Hz, 1H), 7.70 (dd, J = 6.6, 4.4 Hz, 1H), 7.56 (t, J = 5.2 Hz, 2H), 7.44 (t, J = 7.6 Hz, 2H), 7.24 (t, J = 4.8 Hz, 1H), 6.66 (q, J = 12.4 Hz, 2H) ppm. ^{13}C NMR (125 MHz, acetone-d_6): δ 154.2, 154.0, 153.9, 153.6, 153.0, 152.1, 149.3, 149.0, 148.97, 148.9, 139.0, 137.8, 137.7, 137.4, 132.3, 131.99, 131.97, 131.56, 131.5, 131.3, 131.1, 130.2, 129.09, 129.04, 128.9, 128.6, 128.3, 127.1, 126.99, 126.9, 126.8, 126.4, 126.2, 124.2, 123.7, 123.6, 49.0 ppm.

***4*[PF$_6$]$_2$.** Anal. Calcd for $C_{48}H_{32}N_8RuP_2F_{12}$ (M_w = 1112.1077): C, 51.85; H, 2.90; N, 10.08. Found: C, 51.84; H, 2.89; N, 10.04. FTIR in KBr disk (ν/cm^{-1}): 3047, 1620, 1454, 1427, 1344, 1122, 1054, 840, 721. ESI-MS: for $[C_{48}H_{32}N_8RuPF_6]^+$, calcd m/z 967.1430, found m/z 967.1441. ^{1}H NMR (400 MHz, acetone-d_6): δ 9.13 (s, 1H), 8.84 (d, J =8 Hz, 1H), 8.75 (d, J =8 Hz, 1H), 8.64 (d, J =5.6 Hz, 1H), 8.60 (t, J =8.8 Hz, 2H), 8.49 (d, J =5.6 Hz, 1H), 8.46 (d, J =5.2 Hz, 1H), 8.43−8.37 (m, 4H), 8.28 (d, J =8.8 Hz, 2H), 8.23−8.18 (m, 4H), 8.07 (d,, J =8.6 Hz, 1H), 8.03−7.99 (m, 3H), 7.94−7.88 (m, 3H), 7.85−7.81 (m, 2H), 7.77 (dd, J =8, 5.2 Hz, 1H), 7.67 (dd, J =8, 5.2 Hz, 1H), 7.27 (t, J =7.2 Hz, 1H), 6.39 (q, J =14.8 Hz, 2H) ppm. ^{13}C NMR (100 MHz, acetone-d_6): δ 154.2,154.1, 153.9, 153.5, 153.0, 152.2, 149.2, 149.0, 148.9, 148.87, 148.8, 139.1, 137.8, 137.7, 137.6, 137.3, 131.97, 131.96, 131.38, 131.3, 129.27, 129.20, 129.05, 129.0, 128.5, 128.3, 128.2, 127.5, 127.4, 127.1, 126.95, 126.9, 126.8, 126.2, 125.8, 123.6, 122.6, 54.7 ppm.

***5*[PF$_6$]$_2$.** Anal. Calcd for $C_{39}H_{30}ON_8RuP_2F_{12}$ (M_w = 1018.0870): C, 46.03; H, 2.97; N, 11.01. Found: C, 46.02; H, 2.95; N, 10.99. FTIR in KBr disk (ν/cm^{-1}): 3454, 1724, 1514, 1427, 1251, 1178, 842, 775, 723. ESI-MS: for $[C_{39}H_{30}ON_8RuPF_6]^+$, calcd m/z 873.1222, found m/z 873.1227; for $[C_{39}H_{30}ON_8Ru]^{2+}$, calcd m/z 364.0788, found m/z 364.0747. ^{1}H NMR (400 MHz, acetone-d_6): δ 9.07 (s, 1H), 8.86−8.82 (m, 2H), 8.74 (d, J =8.4 Hz, 1H), 8.69 (d, J =8.4 Hz, 1H), 8.60−8.57 (m, 2H), 8.42−8.34 (m, 6H), 8.23 (d, J =5.2 Hz, 1H), 8.06 (t, J =8.2 Hz, 1H), 7.97 (d, J =5.2 Hz, 1H), 7.95 (d, J =5.2 Hz, 1H), 7.85 (d, J =5.2 Hz, 1H), 7.77 (dd, J =8.2, 5.2 Hz, 1H), 7.69 (dd, J =8.2, 5.2 Hz, 1H), 7.30 (t, J =7.2 Hz, 1H), 7.11(d, J =8.4 Hz, 2H), 6.84 (d, J =8.4 Hz, 2H), 5.53 (q, J =14.8 Hz, 2H) ppm. ^{13}C NMR (100 MHz, acetone-d_6): δ 161.1, 154.1, 153.8, 153.1, 152.3, 149.4, 149.2, 149.1, 149.0, 148.9, 139.2, 137.88, 137.8, 137.5, 132.0, 130.7, 129.1, 129.0, 128.8, 127.2, 127.1, 127.0, 126.6, 126.4, 115.2, 55.9, 55.7 ppm.

***6*[PF$_6$]$_2$.** Anal. Calcd for $C_{38}H_{27}O_2N_9RuP_2F_{12}$ (M_w = 1033.0615): C, 44.20; H, 2.64; N, 12.21. Found: C, 44.19; H, 2.61; N, 12.18. FTIR in KBr disk (ν/cm^{-1}): 3411, 3087, 1724, 1604, 1523, 1427, 1346, 1122, 1053, 840, 777, 721. ESI-MS: for $[C_{38}H_{27}O_2N_9RuPF_6]^+$, calcd m/z 888.0968, found m/z 888.0953; for $[C_{38}H_{27}O_2N_9Ru]^{2+}$, calcd m/z 371.5660, found m/z 371.5664. ^{1}H NMR (400 MHz, acetone-d_6): δ 9.35 (s, 1H), 8.85 (t, J =7.6 Hz, 2H), 8.75 (d, J =8.4 Hz, 1H), 8.64 (d, J =8 Hz, 1H), 8.42−8.37 (m, 4H), 8.34−8.28 (m, 3H), 8.15 (d, J =8.4 Hz, 3H), 8.08 (t, J =7.6 Hz, 1H), 8.00−7.93 (m, 3H), 7.74 (dd, J =8, 5.2 Hz, 1H), 7.62 (dd, J =8, 5.2 Hz, 1H), 7.55 (d, J =5.6 Hz, 1H), 7.30 (d, J =8 Hz, 3H), 5.78 (q, J =15.6 Hz, 2H) ppm. ^{13}C NMR (100 MHz, acetone-d_6): δ 152.9, 152.6, 151.7, 150.5, 147.7, 147.6, 147.4, 147.3, 147.2, 147.1, 141.3, 138.2, 137.6, 136.8, 136.4, 130.4, 130.1,

https://doi.org/10.1021/acs.inorgchem.1c01084
Inorg. Chem. 2021, 60, 9084−9096

129.8, 129.1, 127.9, 127.8, 127.6, 126.9, 126.8, 126.3, 125.6, 123.8, 123.7, 122.6, 123.0, 122.9, 53.7 ppm.

7[PF$_6$]$_2$. Anal. Calcd for $C_{34}H_{23}N_8RuP_2F_{17}$ (M_w = 1030.0293): C, 39.66; H, 2.25; N, 10.88. Found: C, 39.64; H, 2.24; N, 10.83. FTIR in KBr disk (ν/cm^{-1}): 3454, 3132, 1604, 1514, 1446, 1357, 1128, 1026, 842, 765, 663. ESI-MS: for $[C_{34}H_{23}N_8RuPF_{11}]^+$, calcd m/z 885.0651, found m/z 885.0647. ^{1}H NMR (500 MHz, DMSO-d_6): δ 9.38 (s, 1H), 8.85 (dd, J =8.5, 3 Hz, 2H), 8.77 (d, J =8 Hz, 1H), 8.74 (d, J =8 Hz, 1H), 8.35 (d, J =8 Hz, 1H), 8.18 (q, J =8 Hz, 3H), 8.13 (t, J =7.9 Hz, 2H), 7.89 (d, J =5.5 Hz, 1H), 7.86 (dd, J =9, 5.5 Hz, 2H), 7.74 (d, J =5.5 Hz, 1H), 7.63 (d, J =6 Hz, 1H), 7.58−7.52 (m, 3H), 7.47 (t, J =7 Hz, 1H), 7.44 (t, J =7 Hz, 1H), 5.86 (s, 2H) ppm.^{13}C NMR (125 MHz, DMSO-d_6): δ 157.2, 156.87, 156.8, 156.5, 151.8, 151.7, 151.6, 151.4, 151.3, 150.1, 147.4, 138.4, 137.98, 137.9, 137.6, 127.7, 127.1, 126.6, 126.4, 124.5, 124.4, 123.9, 123.6, 122.7, 107.9, 42.8 ppm.

■ ASSOCIATED CONTENT

Supporting Information

The Supporting Information is available free of charge at https://pubs.acs.org/doi/10.1021/acs.inorgchem.1c01084.

Detailed syntheses of all ligands and characterization spectra of synthesized compounds, solution-state ^{1}H NMR, X-ray crystallographic data of complexes **1**[PF$_6$]$_2$, **1**[H$_2$PO$_4$]$_2$, **2**[H$_2$PO$_4$]$_2$, **3**[PF$_6$]$_2$, **4**[PF$_6$]$_2$, **4**[H$_2$PO$_4$]$_2$, **5**[PF$_6$]$_2$, **5**[H$_2$PO$_4$]$_2$, **6**[PF$_6$]$_2$,and **7**[PF$_6$]$_2$, solution-state studies (PL, UV, TCSPC, ^{1}H NMR, ^{19}F and ^{31}P) of all probes with anions in solution, solution-state aggregation as well as macroscopic morphological analysis data (PDF)

Accession Codes

CCDC 2048424−2048433 contain the supplementary crystallographic data for this paper. These data can be obtained free of charge via www.ccdc.cam.ac.uk/data_request/cif, or by emailing data_request@ccdc.cam.ac.uk, or by contacting The Cambridge Crystallographic Data Centre, 12 Union Road, Cambridge CB2 1EZ, UK; fax: +44 1223 336033.

■ AUTHOR INFORMATION

Corresponding Author

Pradyut Ghosh − *School of Chemical Sciences, Indian Association for the Cultivation of Science, Kolkata 700032, India;* orcid.org/0000-0002-5503-6428; Email: icpg@iacs.res.in

Authors

Sahidul Mondal − *School of Chemical Sciences, Indian Association for the Cultivation of Science, Kolkata 700032, India*

Koushik Sarkar − *School of Chemical Sciences, Indian Association for the Cultivation of Science, Kolkata 700032, India*

Complete contact information is available at: https://pubs.acs.org/10.1021/acs.inorgchem.1c01084

Notes

The authors declare no competing financial interest.

■ ACKNOWLEDGMENTS

P.G. gratefully acknowledges the Science and Engineering Research Board (SERB; EMR/2016/000900), India, for financial support and the Alexander von Humboldt Foundation for donating a fluorimeter. S.M. gratefully thanks the CSIR for an SRF. The authors especially thank Dr. Bijit Chowdhury, Dr. Tamal Kanti Ghosh, and Dr. Abu Saleh Musha Islam for fruitful discussions during this work.

■ REFERENCES

(1) Nyren, P. Enzymic method for continuous monitoring of DNA polymerase activity. *Anal. Biochem.* **1987**, *167*, 235−8.

(2) Hargrove, A. E.; Nieto, S.; Zhang, T.; Sessler, J. L.; Anslyn, E. V. Artificial Receptors for the Recognition of Phosphorylated Molecules. *Chem. Rev. (Washington, DC, U. S.)* **2011**, *111*, 6603−6782.

(3) Katayev, E. A.; Ustynyuk, Y. A.; Sessler, J. L. Receptors for tetrahedral oxyanions. *Coord. Chem. Rev.* **2006**, *250*, 3004−3037.

(4) Pal, S.; Ghosh, T. K.; Ghosh, R.; Mondal, S.; Ghosh, P. Recent advances in recognition, sensing and extraction of phosphates: 2015 onwards. *Coord. Chem. Rev.* **2020**, *405*, 213128.

(5) Beer, P. D.; Gale, P. A. Anion Recognition and Sensing: The State of the Art and Future Perspectives. *Angew. Chem., Int. Ed.* **2001**, *40*, 486−516.

(6) Hirsch, A. K. H.; Fischer, F. R.; Diederich, F. Phosphate recognition in structural biology. *Angew. Chem., Int. Ed.* **2007**, *46*, 338−352.

(7) Lee, D. H.; Kim, S. Y.; Hong, J.-I. Fluorescent sensors: A fluorescent pyrophosphate sensor with high selectivity over ATP in water. *Angew. Chem., Int. Ed.* **2004**, *43*, 4777−4780.

(8) Schmidtchen, F. P.; Berger, M. Artificial Organic Host Molecules for Anions. *Chem. Rev. (Washington, DC, U. S.)* **1997**, *97*, 1609−1646.

(9) Lee, C.-H.; Na, H.-K.; Yoon, D.-W.; Won, D.-H.; Cho, W.-S.; Lynch, V. M.; Shevchuk, S. V.; Sessler, J. L. Single Side Strapping: A New Approach to Fine Tuning the Anion Recognition Properties of Calix[4]pyrroles. *J. Am. Chem. Soc.* **2003**, *125*, 7301−7306.

(10) Khatua, S.; Choi, S. H.; Lee, J.; Kim, K.; Do, Y.; Churchill, D. G. Aqueous Fluorometric and Colorimetric Sensing of Phosphate Ions by a Fluorescent Dinuclear Zinc Complex. *Inorg. Chem.* **2009**, *48*, 2993−2999.

(11) Gale, P. A. Anion receptor chemistry. *Chem. Commun. (Cambridge, U. K.)* **2011**, *47*, 82−86.

(12) Das, P.; Bhattacharya, S.; Mishra, S.; Das, A. Zn(II) and Cd(II)-based complexes for probing the enzymatic hydrolysis of Na4P2O7 by alkaline phosphatase in physiological conditions. *Chem. Commun. (Cambridge, U. K.)* **2011**, *47*, 8118−8120.

(13) Kim, S. K.; Lee, D. H.; Hong, J.-I.; Yoon, J. Chemosensors for Pyrophosphate. *Acc. Chem. Res.* **2009**, *42*, 23−31.

(14) Tabary, T.; Ju, L.-Y.; Cohen, J. H. M. Homogeneous phase pyrophosphate (PPi) measurement (H3PIM) A non-radioactive, quantitative detection system for nucleic acid specific hybridization methodologies including gene amplification. *J. Immunol. Methods* **1992**, *156*, 55−60.

(15) Marcus, Y. A simple empirical model describing the thermodynamics of hydration of ions of widely varying charges, sizes, and shapes. *Biophys. Chem.* **1994**, *51*, 111−27.

(16) Bowman-James, K. Alfred Werner Revisited: The Coordination Chemistry of Anions. *Acc. Chem. Res.* **2005**, *38*, 671−678.

(17) Gale, P. A.; Garcia-Garrido, S. E.; Garric, J. Anion receptors based on organic frameworks: highlights from 2005 and 2006. *Chem. Soc. Rev.* **2008**, *37*, 151−190.

(18) Ramakrishnam Raju, M. V.; Harris, S. M.; Pierre, V. C. Design and applications of metal-based molecular receptors and probes for inorganic phosphate. *Chem. Soc. Rev.* **2020**, *49*, 1090−1108.

(19) Sturbelle, R. T.; Farias da Costa de Avila, L.; Roos, T. B.; Borchardt, J. L.; de Cassia dos Santos da Conceicao, R.; Dellagostin, O. A.; Leite, F. P. L. The role of quorum sensing in Escherichia coli (ETEC) virulence factors. *Vet. Microbiol.* **2015**, *180*, 245−252.

(20) Kubik, S. Amino acid containing anion receptors. *Chem. Soc. Rev.* **2009**, *38*, 585−605.

(21) Hua, Y.; Flood, A. H. Click chemistry generates privileged CH hydrogen-bonding triazoles: the latest addition to anion supramolecular chemistry. *Chem. Soc. Rev.* **2010**, *39*, 1262−1271.

(22) Garcia-Garrido, S. E.; Caltagirone, C.; Light, M. E.; Gale, P. A. Acridinone-based anion receptors and sensors. *Chem. Commun. (Cambridge, U. K.)* **2007**, 1450−1452.
(23) dos Santos, C. M. G.; McCabe, T.; Gunnlaugsson, T. Selective fluorescent sensing of chloride. *Tetrahedron Lett.* **2007**, *48*, 3135−3139.
(24) Ghosh, T. K.; Chakraborty, S.; Chowdhury, B.; Ghosh, P. Bis-Heteroleptic Ruthenium(II) Complex of Pendant Urea Functionalized Pyridyl Triazole and Phenanthroline for Recognition, Sensing, and Extraction of Oxyanions. *Inorg. Chem.* **2017**, *56*, 5371−5382.
(25) Ghosh, A.; Ganguly, B.; Das, A. Urea-based ruthenium(II)-polypyridyl complex as an optical sensor for anions: synthesis, characterization, and binding studies. *Inorg. Chem.* **2007**, *46*, 9912−9918.
(26) Wu, Y.; Peng, X.; Fan, J.; Gao, S.; Tian, M.; Zhao, J.; Sun, S. Fluorescence Sensing of Anions Based on Inhibition of Excited-State Intramolecular Proton Transfer. *J. Org. Chem.* **2007**, *72*, 62−70.
(27) Chowdhury, B.; Khatua, S.; Dutta, R.; Chakraborty, S.; Ghosh, P. Bis-Heteroleptic Ruthenium(II) Complex of a Triazole Ligand as a Selective Probe for Phosphates. *Inorg. Chem.* **2014**, *53*, 8061−8070.
(28) Zapata, F.; Gonzalez, L.; Caballero, A.; Alkorta, I.; Elguero, J.; Molina, P. Dual Role of the 1,2,3-Triazolium Ring as a Hydrogen-Bond Donor and Anion-π Receptor in Anion-Recognition Processes. *Chem. - Eur. J.* **2015**, *21*, 9797−9808.
(29) Romero, T.; Caballero, A.; Tarraga, A.; Molina, P. A Click-Generated Triazole Tethered Ferrocene-Pyrene Dyad for Dual-Mode Recognition of the Pyrophosphate Anion. *Org. Lett.* **2009**, *11*, 3466−3469.
(30) Schulze, B.; Schubert, U. S. Beyond click chemistry - supramolecular interactions of 1,2,3-triazoles. *Chem. Soc. Rev.* **2014**, *43*, 2522−2571.
(31) Curiel, D.; Cowley, A.; Beer, P. D. Indolocarbazoles: a new family of anion sensors. *Chem. Commun. (Cambridge, U. K.)* **2005**, 236−238.
(32) Yoon, J.; Kim, S. K.; Singh, N. J.; Kim, K. S. Imidazolium receptors for the recognition of anions. *Chem. Soc. Rev.* **2006**, *35*, 355−360.
(33) Molina, P.; Tarraga, A.; Oton, F. Imidazole derivatives: A comprehensive survey of their recognition properties. *Org. Biomol. Chem.* **2012**, *10*, 1711−1724.
(34) Zapata, F.; Caballero, A.; Espinosa, A.; Tarraga, A.; Molina, P. Cation coordination induced modulation of the anion sensing properties of a ferrocene-imidazophenanthroline Dyad: Multichannel recognition from phosphate-related to chloride anions. *J. Org. Chem.* **2008**, *73*, 4034−4044.
(35) Alfonso, M.; Espinosa, A.; Tarraga, A.; Molina, P. A Simple but Effective Dual Redox and Fluorescent Ion Pair Receptor Based on a Ferrocene-Imidazopyrene Dyad. *Org. Lett.* **2011**, *13*, 2078−2081.
(36) Zapata, F.; Caballero, A.; Tarraga, A.; Molina, P. Ferrocene-Substituted Nitrogen-Rich Ring Systems as Multichannel Molecular Chemosensors for Anions in Aqueous Environment. *J. Org. Chem.* **2010**, *75*, 162−169.
(37) Chmielewski, M. J.; Jurczak, J. Anion binding versus intramolecular hydrogen bonding in neutral macrocyclic amides. *Chem. - Eur. J.* **2006**, *12*, 7652−7667.
(38) Hossain, M. A.; Kang, S. O.; Powell, D.; Bowman-James, K. Anion Receptors: A New Class of Amide/Quaternized Amine Macrocycles and the Chelate Effect. *Inorg. Chem.* **2003**, *42*, 1397−1399.
(39) Choi, J. K.; Kim, S. H.; Yoon, J.; Lee, K.-H.; Bartsch, R. A.; Kim, J. S. A PCT-Based, Pyrene-Armed Calix[4]crown Fluoroionophore. *J. Org. Chem.* **2006**, *71*, 8011−8015.
(40) Mondal, S.; Ghosh, K. Naphthalimide-linked bispyridinium clefts in selective aqueous sensing of triphosphate and triphosphate-based biomolecules. *Anal. Methods* **2019**, *11*, 5864−5871.
(41) Fisher, M. G.; Gale, P. A.; Hiscock, J. R.; Hursthouse, M. B.; Light, M. E.; Schmidtchen, F. P.; Tong, C. C. 1,2,3-Triazole-strapped calix[4]pyrrole: a new membrane transporter for chloride. *Chem. Commun. (Cambridge, U. K.)* **2009**, 3017−3019.
(42) Yano, M.; Tong, C. C.; Light, M. E.; Schmidtchen, F. P.; Gale, P. A. Calix[4]pyrrole-based anion transporters with tuneable transport properties. *Org. Biomol. Chem.* **2010**, *8*, 4356−4363.
(43) Park, J.-Y.; Skonieczny, K.; Aratani, N.; Osuka, A.; Gryko, D. T.; Lee, C.-H. Calix[4]pyrroles bearing proximally meso-meso linking straps: synthesis and anion binding properties. *Chem. Commun. (Cambridge, U. K.)* **2012**, *48*, 8060−8062.
(44) Sokkalingam, P.; Hong, S.-J.; Aydogan, A.; Sessler, J. L.; Lee, C.-H. Decoration of Gold Nanoparticles by a Double-Armed Calix[4]pyrrole: A Receptor-Decorated Nanoensemble for Anion Sensing and Extraction. *Chem. - Eur. J.* **2013**, *19*, 5860−5867.
(45) Sokkalingam, P.; Kim, D. S.; Hwang, H.; Sessler, J. L.; Lee, C.-H. A dicationic calix[4]pyrrole derivative and its use for the selective recognition and displacement-based sensing of pyrophosphate. *Chem. Sci.* **2012**, *3*, 1819−1824.
(46) Chowdhury, B.; Dutta, R.; Khatua, S.; Ghosh, P. A Cyanuric Acid Platform Based Tripodal Bis-heteroleptic Ru(II) Complex of Click Generated Ligand for Selective Sensing of Phosphates via C-H··· Anion Interaction. *Inorg. Chem.* **2016**, *55*, 259−271.
(47) Chowdhury, B.; Sinha, S.; Ghosh, P. Selective Sensing of Phosphates by a New Bis-heteroleptic RuII Complex through Halogen Bonding: A Superior Sensor over Its Hydrogen-Bonding Analogue. *Chem. - Eur. J.* **2016**, *22*, 18051−18059.
(48) Ghosh, T. K.; Ghosh, P. Balancing the acidity of the pendant urea arm of bis-heteroleptic ruthenium(II) complex containing pyridyl triazole for improved oxyanion recognition. *Dalton Trans.* **2018**, *47*, 7561−7570.
(49) Ghosh, T. K.; Mondal, S.; Bej, S.; Nandi, M.; Ghosh, P. An integrated urea and halogen bond donor based receptor for superior and selective sensing of phosphates. *Dalton Trans.* **2019**, *48*, 4538−4546.
(50) Mondal, S.; Ghosh, T. K.; Chowdhury, B.; Ghosh, P. Supramolecular Self-Assembly Driven Selective Sensing of Phosphates. *Inorg. Chem.* **2019**, *58*, 15993−16003.
(51) Zapata, F.; Gonzalez, L.; Bastida, A.; Bautista, D.; Caballero, A. Formation of self-assembled supramolecular polymers by anti-electrostatic anion-anion and halogen bonding interactions. *Chem. Commun. (Cambridge, U. K.)* **2020**, *56*, 7084−7087.
(52) Zapata, F.; Gonzalez, L.; Caballero, A.; Bastida, A.; Bautista, D.; Molina, P. Interlocked Supramolecular Polymers Created by Combination of Halogen- and Hydrogen-Bonding Interactions through Anion-Template Self-Assembly. *J. Am. Chem. Soc.* **2018**, *140*, 2041−2045.
(53) Naskar, S.; Dalal, C.; Ghosh, P. Ion-pair coordination driven stimuli-responsive one-dimensional supramolecular helicate. *Chem. Commun. (Cambridge, U. K.)* **2017**, *53*, 2487−2490.
(54) Lakshminarayanan, P. S.; Ravikumar, I.; Suresh, E.; Ghosh, P. Trapped inorganic phosphate dimer. *Chem. Commun. (Cambridge, U. K.)* **2007**, 5214−5216.
(55) Lakshminarayanan, P. S.; Ravikumar, I.; Suresh, E.; Ghosh, P. Encapsulation of Halides within the Cavity of a Pentafluorophenyl-Substituted Tripodal Amine Receptor. *Inorg. Chem.* **2007**, *46*, 4769−4771.
(56) Dutta, R.; Ghosh, P. Encapsulation of Fluoride/Chloride in the C3v-Symmetric Cleft of a Pentafluorophenyl-Functionalized Cyanuric Acid Platform Based Tripodal Amide: Solid and Solution-State Anion-Binding Studies. *Eur. J. Inorg. Chem.* **2012**, *2012*, 3456−3462.
(57) Ravikumar, I.; Lakshminarayanan, P. S.; Arunachalam, M.; Suresh, E.; Ghosh, P. Anion complexation of a pentafluorophenyl-substituted tripodal urea receptor in solution and the solid state: Selectivity toward phosphate. *Dalton Trans.* **2009**, 4160−4168.
(58) Janiak, C. A critical account on $\pi-\pi$ stacking in metal complexes with aromatic nitrogen-containing ligands. *J. Chem. Soc., Dalton Trans.* **2000**, 3885−3896.
(59) Thordarson, P. Determining association constants from titration experiments in supramolecular chemistry. *Chem. Soc. Rev.* **2011**, *40*, 1305−1323.
(60) Brynn Hibbert, D.; Thordarson, P. The death of the Job plot, transparency, open science and online tools, uncertainty estimation

https://doi.org/10.1021/acs.inorgchem.1c01084
Inorg. Chem. 2021, 60, 9084−9096

methods and other developments in supramolecular chemistry data analysis. *Chem. Commun. (Cambridge, U. K.)* **2016**, *52*, 12792−12805.
(61) *SAINT - Software for the Integration of CCD Detector System Bruker Analytical X-ray Systems*; Bruker AXS: Madison, WI, 1995.
(62) Sheldrick, G. M. *SADABS, Empirical Absorption Correction Program*; University of Göttingen: Göttingen, Germany, 1997.
(63) Sheldrick, G. M. *SHELXS97. Program for Crystal Structure Solution and Refinement*; University of Göttingen: Göttingen, Germany, 1997.
(64) Sheldrick, G. M. *SHELXL v. 2014, Program for Crystal Structure Refinement*; University of Göttingen, Göttingen, Germany, 2014.
(65) Spek, A. L. *PLATON-97*; University of Utrecht: Utrecht, the Netherlands, 1997.
(66) *Mercury, version* 3.7, supplied with Cambridge Structural Database, CCDC, Cambridge, U.K., 2003−2004.
(67) Collins, J. E.; Lamba, J. J. S.; Love, J. C.; McAlvin, J. E.; Ng, C.; Peters, B. P.; Wu, X.; Fraser, C. L. Ruthenium(II) α-Diimine Complexes with One, Two, and Three 4,4′-Bis(hydroxymethyl)-2,2′-bipyridine and 4,4′-Bis(chloromethyl)-2,2′-bipyridine Ligands: Useful Starting Materials for Further Derivatization. *Inorg. Chem.* **1999**, *38*, 2020−2024.

https://doi.org/10.1021/acs.inorgchem.1c01084
Inorg. Chem. 2021, 60, 9084−9096